Diamond & Related Materials 135 (2023) 109837

Contents lists available at ScienceDirect

Diamond & Related Materials

journal homepage: www.elsevier.com/locate/diamond

# Comparative determination of atomic boron and carrier concentration in highly boron doped nano-crystalline diamond

Andrew Taylor [a,*], Petr Ashcheulov [a], Pavel Hubík [a], Zdeněk Weiss [a], Ladislav Klimša [a], Jaromír Kopeček [a], Jan Hrabovsky [b,c], Martin Veis [b], Jan Lorinčík [d], Ivan Elantyev [d], Vincent Mortet [a]

[a] FZU - Institute of Physics CAS, Na Slovance 1999/2, 18221 Prague, Czech Republic
[b] Faculty of Mathematics and Physics, Institute of Physics, Division of Magnetooptics, Charles University, Prague, Czech Republic
[c] HiLASE Centre, Institute of Physics, CAS, Dolní Břežany, Czech Republic
[d] Research Centre Rez, 250 68, Husinec-Řež 130, Czech Republic

ARTICLE INFO

*Keywords:*
Diamond
Boron doping
Estimation
Spectroscopic
Relative
Hall

ABSTRACT

We have compared the total boron content and hole carrier concentration values obtained from various destructive and non-destructive quantification methods in boron doped nano-crystalline diamond films prepared over a range of doping levels, using microwave plasma enhanced chemical vapour deposition. Destructive secondary-ion mass spectrometry and relatively unreported glow discharge optical emission spectrometry were complemented by non-destructive Raman, spectroscopic ellipsometry and van der Pauw Hall measurements. Measurement techniques are discussed, including details of the glow discharge optical emission spectrometry technique; use of different laser powers and wavelengths, fitting parameters for Raman spectroscopy, and improved ellipsometry modelling. Finally, measured values are compared and discussed regarding their viability for estimation of total boron and electrically active boron in doped nano-crystalline diamond layers.

## 1. Introduction

In recent decades diamond ($sp^3$-bonded carbon) has been actively studied because of its outstanding properties, which today benefit many industrial applications [1]. In addition, heavily boron (B) doped diamond with metallic type conductivity is acknowledge as one of the best materials for fabrication of electrodes in electrochemical applications, e.g., water treatment [2], chemical sensing [3] or dye sensitized solar cell [4]. Typically, boron doped diamond (single crystal, micro-crystalline or nano-crystalline), is grown from a mix of $H_2$ and $CH_4$ plus the addition of B in the form of trimethylborane (TMB) - $B(CH_3)_3$ or diborane – $B_2H_6$ using microwave plasma enhanced (MW PECVD) [5,6] or hot filament [7,8] chemical vapour deposition techniques with a substrate temperature of 600–1000 °C. Recently, we have reported on the synthesis of boron doped nano-crystalline diamond (BNCD) layers grown utilizing scalable microwave plasma enhanced CVD systems with linear antenna delivery (MW-LA-PECVD) [9].

Measurement of boron concentration, [B], is an important feedback parameter and is typically determined by methods including: secondary ion mass spectroscopy (SIMS) – a destructive, but sensitive and widely accepted relative measurement; Hall van der Pauw (assuming the acceptor concentration is equal to the hole concentration), a non-destructive and widely accepted measurement relevant to possible electronic applications, which requires contact preparation; or Raman spectroscopy a non-destructive, simple and quick technique, but which becomes more complex with increasing non-diamond carbon species, dopants and other impurities. However, Raman has been reported to enable the determination of boron concentration [10]. In our recent work we have demonstrated that atomic boron concentration can be determined either from the width or position of the unperturbed phonon density of states (PDoS) or diamond zone centre phonon (ZCP) lines for heavily doped single crystal diamond [11], in this work we extend this method to BNCD layers. Additionally, spectroscopic ellipsometry (SE) and glow discharge optical emission spectroscopy (GD-OES) are possible alternative techniques. SE is a non-destructive optical technique, which has in-situ capabilities, important for monitoring layer properties during deposition. SE using different approaches and optical models has previously been reported for the ex-situ characterization of the optical

* Corresponding author.
*E-mail address:* taylor@fzu.cz (A. Taylor).

https://doi.org/10.1016/j.diamond.2023.109837
Received 15 December 2022; Received in revised form 3 March 2023; Accepted 4 March 2023
Available online 11 March 2023

properties of BNCD films [9,12,13,14], here we described model parameters which affect the estimation of free carriers in BNCD and presented the most reliable way for SE estimation of hole concentration. Relatively unreported for such samples [15], GD-OES offers another alternative. This destructive, sensitive, matrix independent and quick technique has been used here for the first time to quantitatively analyse such films. Each technique for B estimation has benefits and drawbacks, therefore, here we aim to compare all techniques to highlight differences.

## 2. Experimental

BNCD layers were deposited using an ASTeX 5010 (Seki Technotron, Japan) deposition system with the following conditions: 0.5 % $CH_4$ diluted in $H_2$, gas pressure = 50 mbar, microwave power = 1150 W, substrate temperature ≈ 750 °C and a growth duration = 2.5 h. Boron doping was obtained by the addition of TMB in the gas phase to give B/C ratios of 500, 1000, 1500, 2000, 2500, 3000, 3500 and 4000 ppm. In addition, a multi-layer sample with increasing steps of B/C (60 min for 500 ppm and 45 min for all other steps) across the same range separated by short (15 min) undoped layers was prepared for SIMS and GD-OES analysis. For the deposition of BNCD layers two types of substrates were utilized: high temperature glass (Corning Eagle XG) and conductive silicon substrates (ON Semiconductor Czech Republic s.r.o.). Prior to loading into the deposition chamber, substrates were cleaned in an ultrasonic bath using acetone, isopropyl alcohol, $H_2SO_4/H_2O_2$ and rinsed in DI water. Substrates were then seeded with a nanodiamond dispersion (NanoAmando®B) in water (0.2 g/l) using a spin coater. In addition, just prior to seeding, conductive Si substrates were dipped in a mixture of 1 % HF and 0.1 % HCl (to remove any native oxide layer) and then immediately seeded and placed in the deposition chamber and pumped down to vacuum.

The surface morphology of deposited layers was observed by scanning electron microscopy (SEM) using a Tescan FERA3 tool. Layer thickness of BNCD layers on conductive Si substrates, with cleaved edges, was measured from cross section SEM observations.

Raman spectroscopy was carried out on layers on glass substrates at room temperature using a Renishaw InVia Raman Microscope with a laser spot size of 2 μm at wavelengths of 325 nm (0.2 mW), 488 nm (6.5 mW @ 100 %) and 785 nm (17.0 mW @ 100 %) with varying laser power to assess quality and layer composition. To evaluate the effect of laser power, prior to all measurements, a $BNCD_{4000}$ layer deposited on glass was used. Using neutral density filters, placed in the laser path, the total laser power was varied from 1, 5, 10, 50 and 100 % for 488 nm and 785 nm wavelengths. At 488 nm from 1 to 50 % laser power no changes were observed, however at 100 % an extra peak at cca. 1590 $cm^{-1}$ appeared, see Fig. SI1. This peak is recognised as being the graphitic G peak, indicating that at this laser power there is enough localised heating to enable graphitisation of the diamond surface. This effect was witnessed over various spots, with varying magnitude, however no damage was observed with the Raman microscope (x50 objective). At 785 nm a similar effect was observed, however this time clear damage to the BNCD layer was observed, see Fig. SI1, again this effect was observed over various spots. Therefore, for the Raman apparatus used in this investigation a laser power maximum of 50 % at 488 nm (3 mW) and 785 nm (8 mW) was used to ensure high signal strength without any damage to the BNCD layer, which could in turn affect layer quality and even [B] evaluation. At 325 nm, subtraction of the signal from the glass substrate was necessary to extract the BNCD signal. This is likely due to a combination of a weak diamond signal and decreased transmission in the glass substrate at lower wavelengths, 60 % at 325 nm, than at higher wavelengths, > 90 % at 488 nm [16]. Indeed, at higher wavelengths no significant substrate signal was observed, see Fig. SI2. For determination of boron concentration, the fitting methods described in [10,17,18] were compared.

For electrical measurements Ti (20 nm)/Au (100 nm) triangle contacts were evaporated on BNCD layers on glass substrates in the corners of a square (~10 × 10 $mm^2$). Resistivity and Hall voltage were measured by the differential van der Pauw (vdP) method in a four-point arrangement at room temperature (298 ± 1) K, using a Keithley 6221 current source and two electrometers, a Keithley 6514, with a Keithley 2182A nanovoltmeter, which recorded the voltage difference between the electrometers, together with a Keithley 708B switching matrix. Pulsed (quasi-DC) measuring mode was used to compensate for parasitic thermoelectric signals and short time drifts. A magnetic field of ±0.4 T was applied.

Secondary-ion mass spectrometry depth profiles were obtained using a magnetic sector SIMS IMS-7f (CAMECA). Parameters used for SIMS measurements were the following: primary ion beam O2+ at 10 keV impact energy, 37 Deg impact angle, and 50 nA ion current, raster size 150 um × 150 um, analysed area 63 um diameter, secondary ion acceleration voltage 5 kV, energy window 25 eV, positive polarity of the secondary ions ($^{11}B+$, $^{12}C+$, $^{28}Si+$), mass resolving power 2000. Oxygen flooding at 1.6 × $10^{-6}$ mbar in the analytical chamber was used to mitigate differences in matrix effects between BNCD and single crystal diamond doped with $^{11}B$ at a constant concentration of 1.$10^{21}$ at $cm^{-3}$, which was used as a reference material for calibration of the concentration scale. The depth scale of the profile was calibrated using a SEM BSE image of the cross-sectional lamella for the BNCD part and an ex-situ measurement of the crater depth with a stylus profilometer DektakXT (Bruker), both under assumption of different, but constant sputter rates for the BNCD layer and silicon substrate. The profile at the BNCD /Si interface was manually corrected to remove artificial transitional effects.

Glow discharge optical emission spectroscopy [19], was used to analyse the composition of the BNCD multilayer on conductive Si substrates. In GD-OES the sample is sputtered layer-by-layer in a glow discharge and the emission spectrum of the atomized sample material is recorded as function of time, thereby providing depth-resolved information about the sample composition. Analysis of B-doped diamond by GD-OES was reported in [20], but without information about the methodology used, and in [15], where an approach based on matrix-specific sensitivity factors (the “ICF method”) was used for analytical interpretation of the data. Additionally, undoped diamond like carbon layers were analysed by GD-OES in [21,22]. In this work, a sputter rate-corrected calibration [23] was established for the B-C-Si system, based on B-alloyed steels, B-alloyed Ni alloy, high-Si steels and cast iron (a high C), reference materials. A unique feature of glow discharge excitation is that it is virtually matrix-independent and the relation between sample composition and signal response is the same for a wide range of materials [19]. Calibration functions for boron (B I, λ = 208.96 nm) and carbon (C I, λ = 165.70 nm) are shown in Fig. SI3. Analyses were made using a GDA750 HR spectrometer (Spectruma GmbH., Germany), in a dc discharge in argon, with a 2.5 mm-diameter anode, at 800 V, 15 mA. Further details are reported in our recent paper [24], solely devoted to the methodology of GDOES analyses of doped diamond layers.

SE measurements were carried out using a variable angle Mueller matrix spectroscopic ellipsometer J.A. Woollam Co. RC2 over the spectral range from 0.73 to 4.13 eV (300–1700 nm) and at an angle of incidence from 60 to 70° with 5° steps. The structure of BNCD films for optical analysis was approximated by a model consisting of a single layer on the parameterized semi-infinitive bulk substrate, thick enough to prevent incoherent back-side reflection affecting the acquired spectra. Surface roughness was considered using Bruggeman effective medium approximation (50 % of void and 50 % of BDD) [25]. Parametrized optical constants were obtained on the blank substrate from the same wafer series. Spectral dependence of BNCD electric permittivity was therefore parameterized using three different models. These models combine the sum of Drude and Tauc-Lorentz (TL) terms with respect to the wavelength range. The principal model operates over the whole wavelength range (300–1700 nm) and combines the contribution of inter-band electronic transitions represented by Tauc-Lorentz (1) term

$\varepsilon_{TL}$ (a classical approach to derive the optical constants of single crystal diamond) and the intra-band electronic transitions in the IR spectral range covered by the Drude term (2) [9]. Inter-band electronic transitions occur between σ bands ($sp^3$ hybridized C), π bands ($sp^2$ hybridized C in BDD grain boundaries) or between σ and π [9,26]. Tauc-Lorentz term is then expressed as

$$\varepsilon_{TL}(E) = \varepsilon_{n1} + i\varepsilon_{n2}$$

$$E > E_g : \varepsilon_{n2} = \left[\frac{A_{TL}E_0Br(E-E_g)^2}{(E^2-E_0^2)^2 + Br^2E^2} \bullet \frac{1}{E}\right]$$

$$E \le E_g : \varepsilon_{n2} = 0 \quad (1)$$

where $A_{TL}$ is the amplitude, $E_g$ is the bandgap energy and $Br$ is the spectral broadening. Tauc-Lorentz function can be also used to compare the quality of BNCD layers with optical constants of single crystalline diamond, which does not contain any defect sites, i.e., $sp^2$ hybridized C [9]. In contrary, intra-band electronic transitions in BNCD are mainly caused by the absorption of light by free carriers in the valence band and are described by the Drude term $\varepsilon_D$ (2).

$$\varepsilon_D = \varepsilon_\infty - (A)/(E^2 + iBE) \quad (2)$$

Hence, when a boron atom replaces a para-continue carbon atom and accepts one electron, the free carriers are dominantly represented by free holes. The free hole concentration $N_f$ (3) and mobility $\mu$ (4) can be then derived from two Drude parameters of amplitude $A$ and broadening $B$ using the value of a free hole effective mass of $m^* = 0.3\ m_e$ as follows [27],

$$A = \varepsilon_\infty(\hbar\omega_p)^2 = \varepsilon_\infty\left(\frac{\hbar^2e^2N_f}{\varepsilon_0\varepsilon_\infty m^*}\right) \quad (3)$$

$$B = \frac{\hbar e}{m^*\mu} \quad (4)$$

where $\omega_p$ stands for plasma frequency of collective charge excitation and $\varepsilon_\infty$ is a high frequency permittivity contribution. The second model also considers both Drude and T-L contribution but using a narrower range of wavelengths (400–1700 nm) and thus eliminates the spectral region with the greatest degree of depolarization in the UV part of spectra due to light scattering on the BNCD rough surface. The last model used involves only Drude's contribution and is limited to the wavelength region beyond 800 nm. This last modification can reduce the deviation between the experimental data and the theoretical model, which is mainly expressed by a mismatch between the Tauc's model and experimental data in the UV region with a higher depolarization rate. In contrary, the single crystal diamond reference sample was analysed using only the T-L contribution over the whole spectral range 193–1700 nm (6.42–0.73 eV).

## 3. Results and discussion

SEM investigation, see Fig. 1, confirmed coalesced films with no pinholes and a morphology typical for nano-crystalline diamond with a well-defined grain shape for all selected samples. Layers show the same morphology as reported in [28], which reported a preferential {011} texture along with a contribution from {111}. Thickness measurements from cleaved cross sections taken from the centre of each sample confirmed thicknesses to be in the range typical for BNCD layers, i.e., ~400–500 nm.

Electrical characteristics of samples were investigated by 4-point resistivity and Hall concentration measurement by the vdP method. As the investigated layers were grown on insulating glass substrates characteristics of BNCD films were solely measured. Resistivity values ranged from 0.1 Ω.cm ($BNCD_{500}$) to 0.002 Ω.cm ($BNCD_{4000}$). Carrier concentrations ranged from $0.23 \times 10^{21}$ $cm^{-3}$ ($BNCD_{500}$) to $4.47 \times 10^{21}$ $cm^{-3}$ ($BNCD_{4000}$). These concentrations are very close or above the metal-insulator transition in boron doped diamond [29] therefore we can assume that all boron acceptors are fully ionized in our samples and measured hole concentration values are equal to the net (uncompensated) acceptor concentrations. The acceptor concentration values determined under the above assumption are in the same range as values calculated from Raman, discussed below, which estimates "active" B in the diamond lattice; this suggests that the compensation rate of [B], e.g., by N contamination, in the investigated samples is low.

Fig. 2 shows a GD-OES depth profile of the multi-layer sample, compared with a SIMS profile from the same sample. Boron concentration profiles are matching with a slight difference in the thickness scaling. With respect to the aim of this work, this is an excellent result, where we have a relative comparison of the same sample in a series with a single variable parameter (i.e., boron doping). A remarkable feature of diamond, related to GD-OES, is that it exhibits an extremely low sputtering rate in a glow discharge (lower by a factor of ≈30–50 than that of typical metals). To our knowledge, no other material with a comparably low sputtering rate has so far been reported to be analysed by GD-OES. Quantitative interpretation of our GD-OES data was based on the approximation of matrix-independent emission yields [23]. The thereby supported calibration model has been successfully used in the analysis of a wide range of materials, is widely accepted and produces accurate

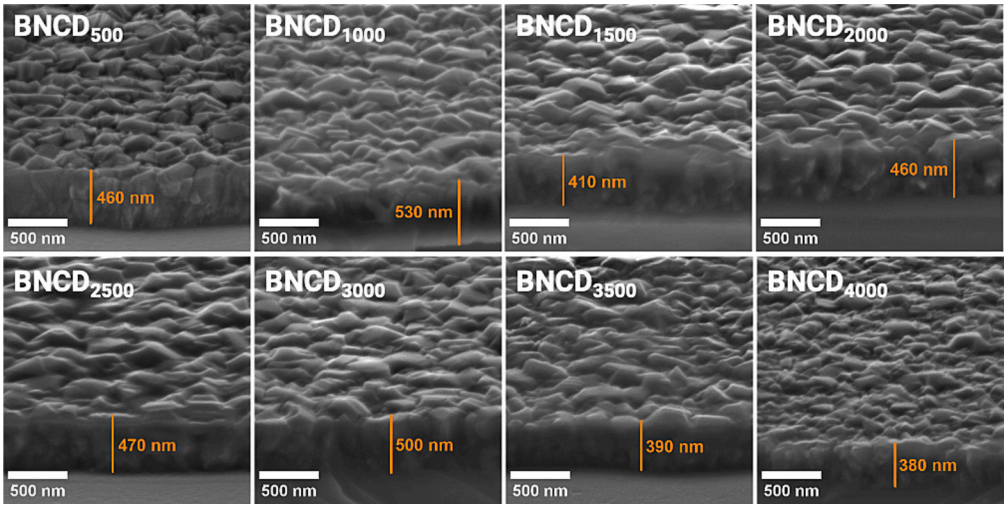


**Fig. 1.** SEM micrographs of cross-sectional views of investigated samples showing BNCD layer thickness and morphology.

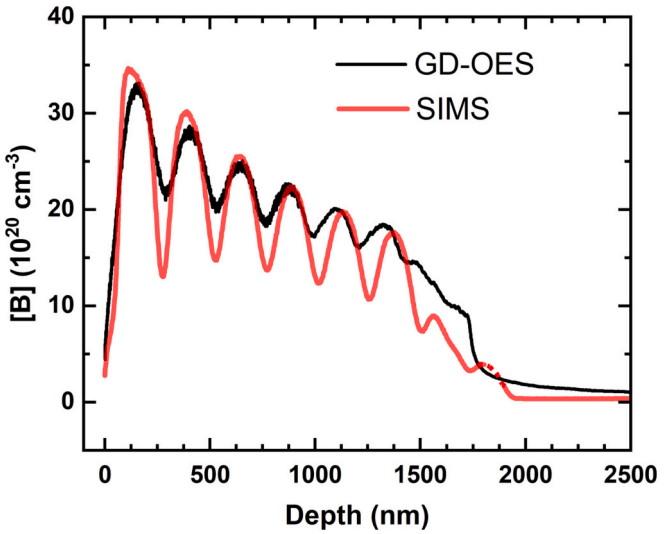


**Fig. 2.** SIMS & GD-OES [B] profiles of BNCD with B/C = 500 to 4 k ppm with undoped interlayers.

results. Nevertheless, it has a semi-empirical character and as such needs to be subjected to extensive testing in any new analytical application. This is typically done by comparison with other methods, while using the concept of metrological traceability [23], including rigorous estimates of the uncertainties associated with such analyses [24].

Raman spectroscopy was initially used for comparison of the three excitation wavelengths, UV (325 nm), visible (488 nm) and infrared (785 nm), across all B/C ratios, see Fig. 3. This revealed that at 325 nm the band at cca. 1530 $cm^{-1}$, is enhanced. This band is also visible at 488 nm, but with lower intensity, whereas at 785 nm it is not present. This band is close to the position identified as trans polyacetylene (TPA) in [30], however the accompanying feature at 1150 $cm^{-1}$ is absent. Moreover, the trend of higher sensitivity to non-diamond carbon as excitation wavelength increases, as reported in [31], is not seen, suggesting that this peak is related to a different effect. A similar effect can also be seen in [32]. B related features at 500, 1250 and shifted 1332 $cm^{-1}$ peak are visible for all wavelengths, sensitivity to B related features increases with laser wavelength, for example in sample $BNCD_{500}$ with 785 nm excitation the 500 and 1250 $cm^{-1}$ peaks are present, whereas at lower wavelengths they are either not well resolved or absent. The combination of bands at ca. 1530 $cm^{-1}$ and the appearance, or not, of B related features is important when considering which fitting method to use to estimate [B].

For comparison of [B] estimated from Raman spectra, three fitting methods were selected: I) Mortet et al. Carbon, (2020) [18], II) Mortet et al. Carbon, (2017) [16] and III) Bernard et al. Diamond and Related Materials Volume, (2004) [10], for each excitation wavelength. For Method I) the fitting tool at [33] was used. This method uses the shift of the position and the broadening of the $sp^3$ peak with increasing defect density (assumed to be exclusively boron in this method) in the diamond. However, other imperfections of the crystal also contribute to the broadening and the shift of the peak, e.g., substitutional nitrogen, vacancies, dislocations, etc. This makes the analysis of BNCD Raman spectrum uncertain as this material is very different from single crystal diamond, on which this model is based, i.e., presence of $sp^2$ carbon, and other crystalline defects, such as twining [34]. Nevertheless, to evaluate the worthiness of this method, fitting was carried out. Two fitting ranges were used a) standard range (1100–1500 $cm^{-1}$) and b) a narrower range (1200–1400 $cm^{-1}$) to reduce any effect from Raman signal at ca. 1525 $cm^{-1}$. The other 2 methods rely solely on the position of the 500 $cm^{-1}$ band, which from a fitting point of view is simpler. Fig. 4 shows the results of these fitting methods, with SIMS values for [B] as a guide, for estimation of [B] for each excitation wavelength. At 325 nm data is rather scattered and does not follow any expected trend for all methods. This is likely due to interference from the 1525 $cm^{-1}$ feature and limited

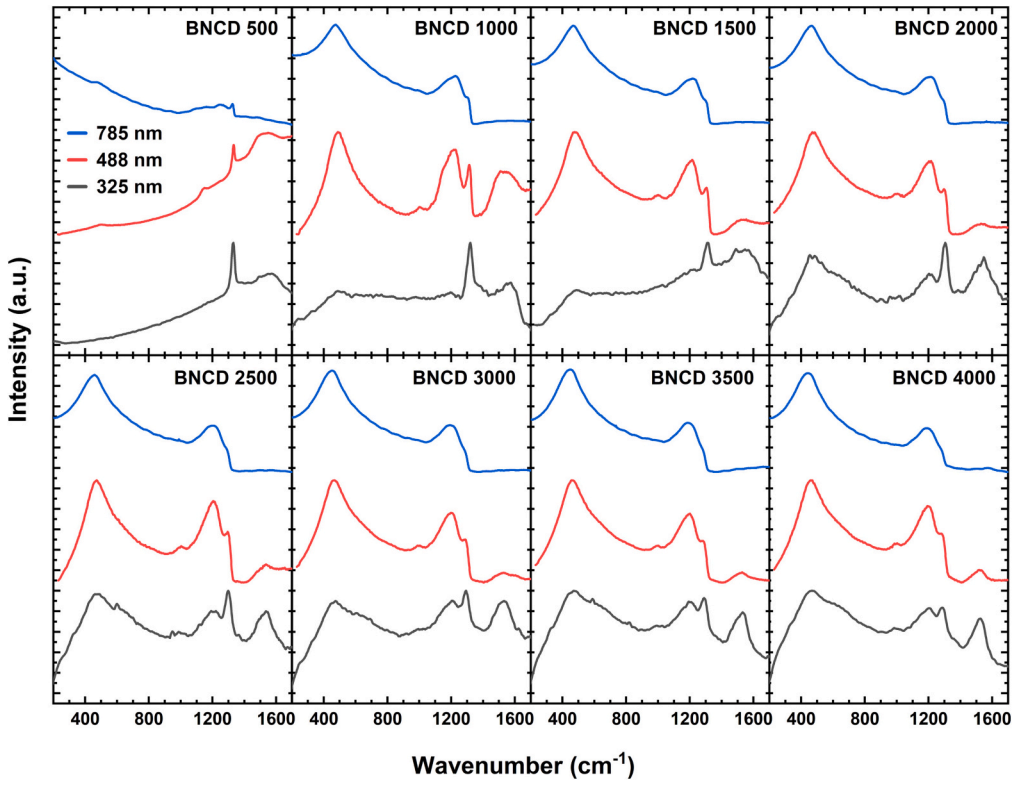


**Fig. 3.** Comparison of 325 (black), 488 (red) and 785 nm (blue) Raman spectra from all investigated samples. (For interpretation of the references to colour in this figure legend, the reader is referred to the web version of this article.)

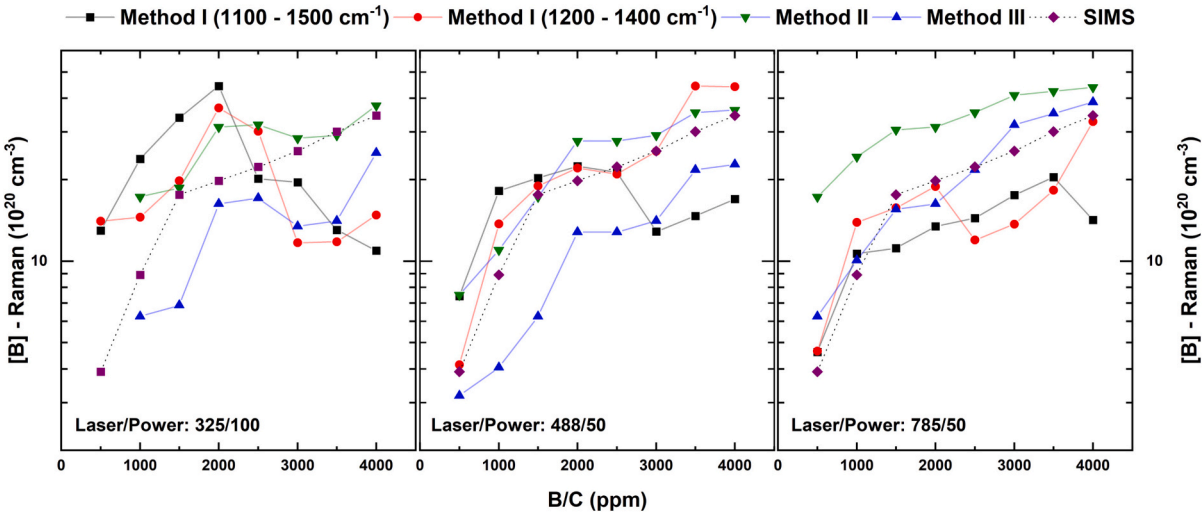


**Fig. 4.** Comparison of Raman fitting methods used for [B] estimation with 325 nm excitation (left) 488 nm excitation @ 50 % laser power (centre) and 785 nm excitation @ 50 % laser power (right).

B related features in comparison with other excitation wavelengths. At 488 nm Method I) initially provides data which does not follow the trend of II) and III) both of which follow the same trend, especially at high B/C. However, when the fitting range is reduced, and therefore reduces the signal from supposedly non-diamond carbon, but not entirely removed, e.g., there could still be a hidden contribution from any graphitic D peaks at 1350 $cm^{-1}$ and TPA at 1150 $cm^{-1}$, [B] follows the same trend as Method II) and Method III) indicating the quality of the fitting carried out. At 785 nm [B] values calculated from Method I) do not follow the trends seen in Method II) Method and III), this could be due to the strong contribution of PDoS compared to ZCP line. Using the SIMS [B] values as a guide, it can be seen that 488 nm excitation provides a narrower spread of values from all methods, and from these Method I) with the narrower range (1200–1400 $cm^{-1}$) gives the most consistent results, i.e., increase in [B] with B/C without large deviations close to SIMS values up to B/C = 3000 ppm. Whereas [B] values estimated from Method II) and Method III) are consistently higher or lower, respectively. Therefore, Method I) with the narrower range with 488 nm excitation was used for comparison with all other techniques.

Spectroscopic ellipsometry as the second non-destructive method was used to determine the concentration of free carriers in BNCD films. Derived optical properties using all three models on the BNCD samples are shown in Fig. 5 in the form of spectral dependence of extinction coefficient. Optical parameters of single crystal diamond (n and k) are included in Fig. SI4 and Tab. SI1. Obtained parameters of Drude and T-L terms of the principal model are listed in Table 1. The first important observation shows us that the dependence of the observed free carrier concentrations follows the same trend as the other complementary techniques used. Thus, as the B/C ratio increases, the BNCD layers show increasing absorption (Drude term amplitude) in the IR part of spectra. This absorption is related to an increase in free hole density and therefore naturally with the concentration of uncompensated boron. However, compared to other techniques, a certain degree of saturation can be observed for higher B/C ratio values. This saturation was observed for all three models used, which can be caused by higher optical absorption in the layers with higher B/C ratio and then decreasing value of light

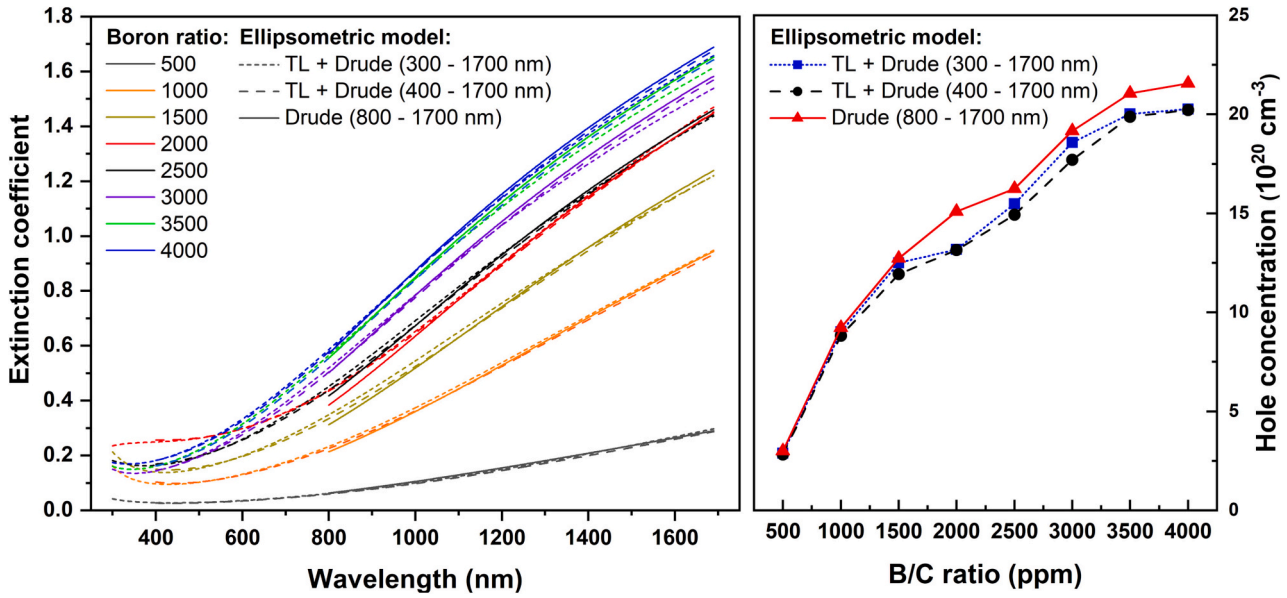


**Fig. 5.** Spectral dependence of extinction coefficient as a function of B/C ratio (left) and the concentration of free carriers to B/C ration with respect to the ellipsometry model used (right).

**Table 1**
Ellipsometry model parameters of BNCD samples using the Tauc-Lorentz and Drude approximation over the spectral range 300–1700 nm. Values marked by * were fixed to control the fit on the values determined for undoped and doped BDD films [9].

| | Tauc-Lorentz | | | | Drude | | | Model parameters | | | |
|---|---|---|---|---|---|---|---|---|---|---|---|
| | $A_{TL}$ | $Br$ | $E_g$ | $E_0$ | $\varepsilon_\infty$* | $A$ | $B$ | $Ep$ | Thickness | Roughness | MSE |
| | eV | eV | eV | eV | | eV$^2$ | eV | eV | nm | nm | |
| $BNCD_{500}$ | 8.11 | 0.82 | ~ 0 | 7.01 | 3 | 1.33 | 0.88 | 0.67 | 559 | 16.8 | 26.7 |
| $BNCD_{1000}$ | 4.79 | 1.97 | ~ 0 | 5.78 | 3 | 4.14 | 1.14 | 1.18 | 473 | 16.3 | 25.2 |
| $BNCD_{1500}$ | 3.50 | 2.74 | ~ 0 | 5.35 | 3 | 5.74 | 1.30 | 1.38 | 452 | 16.0 | 25.5 |
| $BNCD_{2000}$ | 5.01 | 6.56 | ~ 0 | 4.86 | 3 | 6.06 | 1.05 | 1.42 | 375 | 13.3 | 19.3 |
| $BNCD_{2500}$ | 4.18 | 5.05 | ~ 0 | 6.12 | 3 | 7.12 | 1.36 | 1.54 | 466 | 16.0 | 22.1 |
| $BNCD_{3000}$ | 4.37 | 2.70 | ~ 0 | 6.31 | 3 | 8.54 | 1.53 | 1.69 | 428 | 17.8 | 19.6 |
| $BNCD_{3500}$ | 4.93 | 3.54 | ~ 0 | 6.66 | 3 | 9.20 | 1.55 | 1.75 | 403 | 17.9 | 16.3 |
| $BNCD_{4000}$ | 5.60 | 5.89 | ~ 0 | 7.19 | 3 | 9.32 | 1.52 | 1.76 | 408 | 17.7 | 15.5 |
| Single crystal | 292.4 | 3.45 | 5.58 | 9.93 | – | – | – | – | Bulk | 3.69 | 3.40 |

penetration depth, see Fig. SI5. Light is therefore absorbed in the volume of the sample and information is only obtained from the near surface region. This issue can thus be compensated by preparing samples of lower thickness. Moreover, the incorporation of boron in diamond is known to cause a shift in the UV part of diamond absorption edge and then influences the parameters of the Tauc-Lorentz oscillator. Together with the thin nanocrystalline nature of the investigated samples and the associated depolarization in the UV, see Fig. SI6, fitting with the principal model (TL + Drude: 300–1700 nm) obtained values exhibiting higher MSE values in the range between 15.5 and 26.7 compared to the reference single crystal diamond, 3.40. Therefore, the fitted spectral range was first reduced by the part with the highest degree of depolarization (TL + Drude: 400–1700 nm) and then further into the IR, considering only the Drude contribution (Drude: 800–1700 nm). These model updates achieved a better fit between the measured data and the model used, while maintaining consistency between the obtained data for free hole concentration and mobility (see Fig. 5 & Tab. SI2). From this it can be concluded that the uncertainty in the model is mainly due to the contribution in the UV region, but most importantly this does not affect the ellipsometry determination of the free carrier concentration. In comparison with other work [9], it is thus clear that not fixing the parameters of the model using TL a Drude contribution does not have a significant effect on obtaining the values of the investigated parameters of free hole concentration and their mobility. Considering the above-mentioned, values calculated from the principal model are used as a comparison for other methods. The only fixed parameter in the models used is the value of high frequency permittivity contribution which is $\varepsilon_\infty = 3$ for models including T-L term and $\varepsilon_\infty = 4$ for model with only assumed Drude contribution [27,35]. Spectra of refractive index are Kramers–Krönig related (not shown) with extinction coefficient. Samples with low boron content ($BNCD_{500}$) have higher refractive index and their value reached 2.24 (600 nm). Since the optical parameters of Tauc-Lorentz oscillator does not vary dramatically (except for the sample with the lowest B concentration) we can conclude that the diamond quality is consistent for all samples and increases with the observed reducing absorption in the visible and UV parts. As the TL oscillator reached values of $E_g$ close to zero and then converge to the form of a classical Lorentz oscillator, we can then conclude that samples with high B/C exhibit metallic character, as was also observed in the previous van de Pauw measurements. Free hole concentration and their mobilities derived from the Drude term are summarised in Table 1.

When comparing all techniques described above for [B] or hole concentration in BNCD, see Fig. 6 and Tab. SI3, we can see that all methods follow the same trend as B/C increases and that values are rather consistent across all methods. At the lowest B/C, values for [B] have the widest spread, suggesting limitations in sensitivity, i.e., increase in errors, for some methods.

SE using refined modelling methods, systematically, gives values for hole concentration lower than SIMS and other methods. However, the SE models used show good agreement between each other and therefore

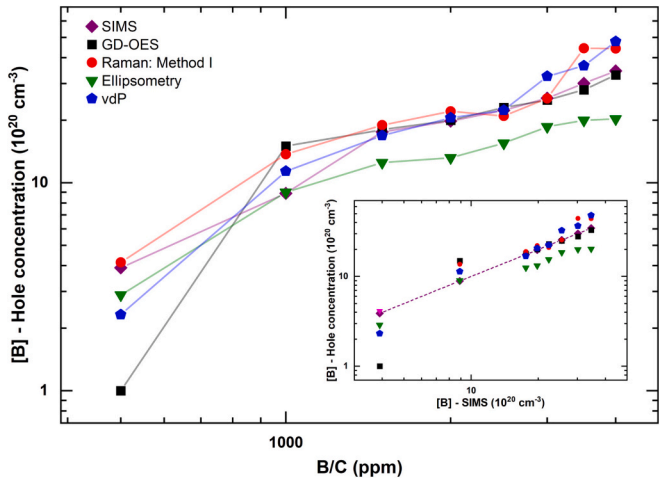


**Fig. 6.** Comparison of all techniques used for [B] / Hole concentration in BNCD grown with B/C from 500 to 4000 ppm. Insert shows values versus SIMS to highlight any non-linearity.

a high degree of universality compared to, for example, the results of B concentration estimated from Raman spectra with different fitting methods.

For Raman spectroscopy it should be considered that this technique measures the quantity of a defect or defects, i.e., defects other than B can contribute to the Raman signal. This contribution, therefore, can lead to a higher estimation of specific defects [17,36]. So, when comparing Raman with other techniques we should consider that we are comparing B related Raman features, which may consist of contribution from electrically active B and non-electrically active B along with an unknown contribution from other defects. Therefore, the [B] estimation from Raman may indeed be higher than vdP and if we consider non-diamond defects, the effect could even be higher than SIMS and/or GD-OES.

Regarding the choice of fitting method, Method I) (488 nm) was chosen as it gave the most consistent results, up to B/C = 3000 ppm, with [B] values close to that of other techniques. If we compare Method II) and Method III) (488 nm), which both use the position of the 500 cm$^{-1}$ band, we can see that Method III) gives consistently low values, whereas Method II) gives high values, suggestion that both may either over or underestimate the true [B] value.

The influence of boron at grain boundaries should also be considered but is a complex and unresolved problem. From the Raman spectra we may estimate the sp$^2$ content to be ~1 %. If we take this value as a measure of grain boundary volume and assume that B incorporation in the grain boundary is comparable with that in the grain bulk [37], the low sp$^2$ content suggests that the total contribution from B in the grain

boundaries is very low. Even if each method has a different sensitivity to boron in grain boundaries, we can roughly estimate that the grain boundary effects will also be of the order of 1 % of the acquired signal. Such a value is smaller than typical measurement errors, which are discussed in detail below. Therefore, in the samples reported here it is unlikely that the effect of boron at the grain boundaries would be observed. For example, at medium B/C range in Fig. 6 we see that Raman, vdP, SIMS and GD-OES give similar values, which may indicate that the quality of the BNCD layers is high, i.e., non-active [B] in grain boundaries and/or defects has minimal effect on the Hall effect measured. Such behavior is possible only if the grain boundary has higher or comparable resistance than the grain itself [38]. This strongly differs from the grain boundary electrical properties observed in ultra-nanocrystalline diamond [39].

Finally, we should consider the accuracy of each method. For SIMS, based on counting statistics, the uncertainty (1-sigma precision) was ~1 %. However, data can be subjected to a systematic deviation from the "true" values due to differences in the matrices between the calibration single crystal diamond sample and the analysed sample. To determine this deviation a new reference with the same matrix would be required, but even if this is produced by implantation of a known [B], there is still open questions relating to the difference in uptake of boron in BNCD, e.g., at grain boundaries and defect sites, between implantation and MW PECVD processes, which should be taken into account when comparing SIMS values for [B] to other methods for the reference.

For SE the variability of the *A* parameter in the Drude model, from which the hole concentration is estimated, analysis shows that any error is within the displayed data points. Errors in Hall concentration measurement include systematic errors of the vdP method due to contact finite size and contact off-edge position. Finite element simulations indicate that these errors make the measured concentration higher than their "true" value and can reach, depending on sample mobility, up to 6 % for the contact geometry used in this case. Furthermore, random errors in Hall constant measurement should be considered, which have been established, using statistic evaluation, as being ~5 %. Additionally, even though alternating current pulses have been used to suppress parasitic thermoelectric effects and instrument errors, at very low Hall voltages, < 0.1 μV, which are below the absolute instrument error range, 0.5 μV, systematic voltmeter errors can occur. Therefore, the total error in Hall concentration has been estimated as 8–20 %, with the upper limit corresponding to the lowest measured voltages, i.e., for samples with the highest B doping levels.

Concerning any uncertainty in GD-OES data, Fig. 6 shows a good correlation with the other methods, except for the lowest point at 500 ppm B/C. This data point comes from a depth of >2000 nm, where a tail in the data, which is caused by contribution from simultaneous sputtering of the shallower depths at the rim of the erosion crater. Overall, there is no concern regarding noise and counting statistics, as the acquired signal was high. Therefore, any possible errors would largely be due to a systematic deviation from the calibration function. Although GD-OES is not matrix dependant, there might still be a matrix effect, i.e., a slightly different response from BNCD than from the ferrous reference samples used in calibration measurements. Usually, work involving the same matrices for calibration and investigated sample, quote a relative error of <3 %, therefore here we may increase this possible error up to ~10 %. Possible errors from Raman spectra acquisition and fitting are also low. However, the chosen method for comparison, Method I) with 488 nm excitation and a narrow fitting range, highlights the need for improvement in the fitting parameters for estimation of [B] at high boron doping levels, due to the weakly pronounced and/or poorly resolved ZCP peak. Therefore, optimum Raman acquisition, e.g., excitation wavelength, and fitting conditions are needed for improved [B] estimation of highly doped BNCD.

Finally, to highlight the validity of the above discussed comparison we should compare the values for hole concentration obtained by vdP with all others. If we assume full ionisation, no compensation and measurement error, [B] values obtained from SIMS and GD-OES should follow the trend and not fall below this threshold as the value for active boron acceptors cannot be higher than the total [B]. Fig. SI7 shows that for $<\sim 2.0 \times 10^{21}$ cm$^{-3}$ this is the case, however at $>\sim 2.0 \times 10^{21}$ cm$^{-3}$ we can see values below the threshold. As discussed above, these anomalies may be corrected using improved reference matrixes for both, and/or improved vdP measurements, assuming over estimation of the values reported due to the discussed possible errors. As mentioned previously, clearly the ellipsometry model requires further optimization. Values estimated from Raman Method I) with 488 nm excitation and a narrow fitting range can be seen to be accurate for determining hole concentrations, with some scatter at $>\sim 2.0 \times 10^{21}$ cm$^{-3}$ indicating that improvements in the fitting may be required.

## 4. Conclusion

BNCD layers have been prepared with varying [B] - hole concentrations. Samples were investigated with various common and rare, destructive, and non-destructive techniques, using relative, calibrated and/or fitting/modelling techniques to extract values. Glow discharge-optical emission spectroscopy was demonstrated for the first time over a range of B/C to give values following the same trend as secondary ions mass spectroscopy. Raman spectroscopy was studied in detail to highlight importance of choice of excitation conditions and fitting method, showing that up to moderate doping levels, fitting of the shift of the position and the broadening of the $sp^3$ peak gives acceptable values. Modelling used in spectroscopic ellipsometry was extended to improve models used for hole concentration estimation, which closely matched values from vdP. Overall, considering possible errors and different contributions, values for [B] estimated from SIMS, GD-OES, Raman and vdP give consistent results. This suggests that spectroscopic ellipsometry could benefit from a suitably chosen standard that would possibly adjust the method offset and further benefit from the versatility of the models used, which give consistent results when changing the fitting parameters. Finally, it can be said that all demonstrated methods have advantages and disadvantages, e.g., simplicity or complexity, destructive or non-destructive, which should be considered depending on when/how/why the [B] - hole concentration values are required.

## CRediT authorship contribution statement

**Andrew Taylor:** Writing – original draft, Writing – review & editing, Investigation, Funding acquisition. **Petr Ashcheulov:** Investigation. **Pavel Hubík:** Investigation, Writing – review & editing. **Zdeněk Weiss:** Investigation, Visualization, Writing – review & editing. **Ladislav Klimša:** Investigation, Visualization. **Jaromír Kopeček:** Investigation. **Jan Hrabovsky:** Investigation, Visualization, Writing – review & editing. **Martin Veis:** Writing – review & editing. **Jan Lorinčík:** Investigation, Visualization, Writing – review & editing. **Ivan Elantyev:** Investigation. **Vincent Mortet:** Conceptualization, Investigation, Writing – review & editing.

## Declaration of competing interest

The authors declare that they have no known competing financial interests or personal relationships that could have appeared to influence the work reported in this paper.

## Data availability

Data will be made available on request.

## Acknowledgements

The Czech Science Foundation [project 20-03187S], Czech Ministry of Education, Youth and Sports projects SOLID21 CZ.02.1.01/0.0/0.0/

16_019/0000760 and CzechNanoLab Research Infrastructure LM2018110, European Regional Development Fund and the state budget of the Czech Republic (project BIATRI: No. CZ.02.1.01/0.0/0.0/15_003/0000445 are gratefully acknowledged. J.H. acknowledges support of the grant SVV-2020-260590. M.V. acknowledges support from grant of Czech Ministry of Education, Youth and Sports No. LTAUSA18176. SIMS has been carried out within the Institutional Support by the Ministry of Industry and Trade of the Czech Republic.

## Appendix A. Supplementary data

Supplementary data to this article can be found online at https://doi.org/10.1016/j.diamond.2023.109837.

## References

[1] R.J. Nemanich, J.A. Carlisle, A. Hirata, K. Haenen, CVD diamond research, applications, and challenges, MRS Bull. 39 (2014) 490–494.
[2] J.V. Macpherson, A practical guide to using boron doped diamond in electrochemical research, Phys. Chem. Chem. Phys. 17 (2015) 2935–2949.
[3] J.H.T. Luong, K.B. Male, J.D. Glennon, Boron-doped diamond electrode: synthesis, characterization,functionalization and analytical applications, Analyst 134 (2009) 1965–1979.
[4] N. Wachter, C. Munson, R. Jarošová, I. Berkun, T. Hogan, R.C. Rocha-Filho, G. M. Swain, Structure, electronic properties, and electrochemical behavior of a boron-doped diamond/quartz optically transparent electrode, ACS Appl. Mater. Interfaces 8 (2016) 28325–28337.
[5] M. Nesládek, D. Tromson, C. Mer, P. Bergonzo, P. Hubik, J.J. Mares, Superconductive B-doped nanocrystalline diamond thin films: electrical transport and Raman spectra, Appl. Phys. Lett. 88 (2006), 232111.
[6] W. Gajewski, P. Achatz, O.A. Williams, K. Haenen, E. Bustarret, M. Stutzmann, J. A. Garrido, Electronic and optical properties of boron-doped nanocrystalline diamond films, Phys. Rev. B 79 (2009), 045206.
[7] J. Zhang, J.W. Zimmer, R.T. Howe, R. Maboudian, Characterization of boron-doped micro- and nanocrystalline diamond films deposited by wafer-scale hot filament chemical vapour deposition for MEMS applications, Diam. Relat. Mater. 17 (2008) 23–28.
[8] Z.L. Wang, Q. Luo, L.W. Liu, C.Y. Li, H.X. Yang, H.F. Yang, J.J. Li, X.Y. Lu, Z.S. Jin, L. Lu, C.Z. Gu, The superconductivity in boron-doped polycrystalline diamond thick films, Diam. Relat. Mater. 15 (2006) 659–663.
[9] A. Taylor, L. Fekete, P. Hubík, A. Jager, P. Janíček, V. Mortet, J. Mistrík, J. Vacík, Large area deposition of boron doped nano-crystalline diamond films at low temperatures using microwave plasma enhanced chemical vapour deposition with linear antenna delivery, Diam. Relat. Mater. 47 (2014) 27–34.
[10] M. Bernard, A. Deneuville, P. Muret, Non-destructive determination of the boron concentration of heavily doped metallic diamond thin films from Raman spectroscopy, Diam. Relat. Mater. 13 (2004) 282.
[11] V. Mortet, Z. Vlčková Živcová, A. Taylor, M. Davydova, O. Frank, P. Hubík, J. Lorincik, M. Aleshin, Determination of atomic boron concentration in heavily boron-doped diamond by Raman spectroscopy, Diam. Relat. Mater. 93 (2019) 54–58.
[12] A. Zimmer, O.A. Williams, K. Haenen, H. Terryn, Optical properties of heavily boron-doped nanocrystalline diamond films studied by spectroscopic ellipsometry, Appl. Phys. Lett. 93 (2008), 131910.
[13] S. Gupta, A. Dudipala, O.A. Williams, K. Haenen, E. Bohannan, Ex situ variable angle spectroscopic ellipsometry studies on chemical vapor deposited boron-doped diamond films: layered structure and modeling aspects, J. Appl. Phys. 104 (2008), 073514.
[14] M. Sobaszek, Ł. Skowronski, R. Bogdanowicz, K. Siuzdak, A. Cirocka, M. Gnyba, M. Naparty, P. Zie˛ba, Ł. Gołuński, P. Płotka, Optical and electrical properties of ultrathin transparent nanocrystalline boron-doped diamond electrodes, Opt. Mater. 42 (2015) 24–34.
[15] D.K. Sharma, A.V. Girão, P. Chapon, M.A. Neto, F.J. Oliveira, R.F. Silva, Advances in RF glow discharge optical emission spectrometry characterization of intrinsic and boron-doped diamond coatings, ACS Appl. Mater. Interfaces 14 (2022) 7405–7416.
[16] https://www.corning.com/media/worldwide/cdt/documents/EAGLE%20XG_PI%20Sheet_2021.pdf.
[17] V. Mortet, Z.V. Zivcova, A. Taylor, O. Frank, P. Hubik, D. Tremouilles, F. Jomard, J. Barjon, L. Kavan, Insight into boron-doped diamond raman spectra characteristic features, Carbon 115 (2017) 279–284.
[18] V. Mortet, I. Gregora, A. Taylor, N. Lambert, P. Ashcheulov, Z. Gedeonova, P. Hubik, New perspectives for heavily boron-doped diamond Raman spectrum analysis, Carbon 168 (2020) 319–327.
[19] V. Hoffmann, A. Quentmeier, in: G. Friedbacher, H. Bubert (Eds.), Glow Discharge Optical Emission Spectroscopy (GD-OES), in Surface and Thin Film Analysis: A Compendium of Principles, Instrumentation and Applications, 2nd edn, Wiley-VCH Verlag GmbH & Co. KGaA, Weinheim, 2011.
[20] T. Watanabe, T.K. Shimizu, Y. Tateyama, Y. Kim, M. Kawai, Y. Einaga, Giant electric double-layer capacitance of heavily boron-doped diamond electrode, Diam. Relat. Mater. 19 (2010) 772–777.
[21] C. Schubert, V. Hoffmann, A. Kümmel, J. Sinn, M. Härtel, A. Reuther, M. Thomalla, T. Gemming, J. Eckert, C. Leyense, Compositional depth profiling of diamond-like carbon layers by glow discharge optical emission spectroscopy, J. Anal. At. Spectrom. 31 (2016) 2207–2212.
[22] H. Takahara, R. Ishigami, K. Kodama, A. Kojyo, T. Nakamura, Y. Oka, Hydrogen analysis in diamond-like carbon by glow discharge optical emission spectroscopy, J. Anal. At. Spectrom. 31 (2016) 940–947.
[23] Z. Weiss, Calibration methods in glow discharge optical emission spectroscopy: a tutorial review, J. Anal. At. Spectrom. 30 (2015) 1038–1049.
[24] Z. Weiss, P. Ashcheulov, N. Lambert, A. Taylor, J. Lorincik, M. Kil-dong Sung, V. Mortet Davydova, Analysis of boron- and phosphorus-doped diamond layers by glow discharge optical emission spectroscopy in argon and neon, Vacuum 111890 (2023), https://doi.org/10.1016/j.vacuum.2023.111890.
[25] D.A.G. Bruggeman, Berechnung verschiedener physikalischer Konstanten von heterogenen Substanzen. I. Dielektrizitätskonstanten und Leitfähigkeiten der Mischkörper aus isotropen Substanzen, Ann. Phys. 416 (1935) 636–664, https://doi.org/10.1002/andp.19354160705.
[26] M. Nesládek, K. Meykens, L. Stals, M. Vaněček, J. Rosa, Origin of characteristic subgap optical absorption in CVD diamond films, Phys. Rev. B 54 (1996) 5552, https://doi.org/10.1103/PhysRevB.54.5552.
[27] H. Fujiwara, in: Reflection and Transmission of Light, Spectrosc. Ellipsom. Princ. Appl, 2007, pp. 32–48 (accessed May 20, 2022), https://www.wiley.com/enus/Spectroscopic+Ellipsometry%3A+Principles+and+Applications-p-9780470016084.
[28] M. Zelenský, J. Fischer, S. Baluchová, L. Klimša, J. Kopeček, M. Vondráček, L. Fekete, J. Eidenschink, F.M. Matysik, S. Mandal, O.A. Williams, M. Hromadová, V. Mortet, K. Schwarzová-Pecková, A. Taylor, Chem-mechanical polishing influenced morphology, spectral and electrochemical characteristics of boron doped diamond, Carbon 203 (25) (January 2023) 363–376.
[29] T. Klein, P. Achatz, J. Kacmarcik, C. Marcenat, F. Gustafsson, J. Marcus, E. Bustarret, J. Pernot, F. Omnes, B.E. Sernelius, C. Persson, A.F. da Silva, C. Cytermann, Metal-insulator transition and superconductivity in boron-doped diamond, Phys. Rev. B 75 (2007), 165313, https://doi.org/10.1103/PhysRevB.75.165313.
[30] A. C. Ferrari J. Robertson . Origin of the 1150-cm-1 Raman mode in nanocrystalline diamond. Phys.Rev.B, VOLUME 63, 121405(R).
[31] A.C. Ferrari, J. Robertson, Raman spectroscopy of amorphous, nanostructured, diamond–like carbon, and nanodiamond, Philos. Trans. R. Soc. A 362 (2004) 2477–2512, https://doi.org/10.1098/rsta.2004.1452.
[32] P.W. May, W.J. Ludlow, M. Hannaway, P.J. Heard, J.A. Smith, K.N. Rosser, Raman and conductivity studies of boron-doped microcrystalline diamond, facetted nanocrystalline diamond and cauliflower diamond films, Diam. Relat. Mater. 17 (2008) 105–117.
[33] http://ofm.fzu.cz/cs/raman-tool.
[34] Y.G. Lu, S. Turner, J. Verbeeck, S.D. Janssens, P. Wagner, K. Haenen, G. Van Tendeloo, Direct visualization of boron dopant distribution and coordination in individual chemical vapor deposition nanocrystalline B-doped diamond grains, Appl. Phys. Lett. 101 (2012), 041907, https://doi.org/10.1063/1.4738885.
[35] J. Mistrik, P. Janicek, A. Taylor, F. Fendrych, L. Fekete, A. Jager, M. Nesladek, Spectroscopic ellipsometry characterization of nano-crystalline diamond films prepared at various substrate temperatures and pulsed plasma frequencies using microwave plasma enhanced chemical vapor deposition apparatus with linear antenna delivery, Thin Solid Films 571 (2014) 230–237, https://doi.org/10.1016/J.TSF.2014.10.071.
[36] S. Prawer, R. Nemanich, Raman spectroscopy of diamond and doped diamond, Philos. Trans. R. Soc. Lond. A 362 (2004) 2537–2565.
[37] S. Turner, Y. Lu, S.D. Janssens, F. Da Pieve, D. Lamoen, J. Verbeeck, K. Haenen, P. Wagner, G. Van Tendeloo, Local boron environment in B-doped nanocrystalline diamond films, Nanoscale 4 (2012) 5960, https://doi.org/10.1039/c2nr31530k.
[38] J.W. Orton, M.J. Powell, The Hall effect in polycrystalline and powdered semiconductors, Rep. Prog. Phys. 43 (1980) 1263–1307, https://doi.org/10.1088/0034-4885/43/11/001.
[39] N. Wiora, M. Mertens, K. Brühne, H.-J. Fecht, I.C. Tran, T. Willey, A. van Buuren, J. Biener, J.-S. Lee, Grain boundary dominated electrical conductivity in ultrananocrystalline diamond, J. Appl. Phys. 122 (2017), https://doi.org/10.1063/1.4993442.